Post-Buckling Behavior of Variable-Arc-Length Pipe due to Internal Fluid Motion

Wichawat Nathabumrung[1] Panithan Padthomfang[1] Tanakorn Tima[1] and Karun Klaycham[2,*]

[1]Student, Department of Civil Engineering, Faculty of Engineering at Kamphaeng Saen, Kasetsart University, Nakhon Pathom, Thailand
[2] Lecturer, Department of Civil Engineering, Faculty of Engineering at Kamphaeng Saen, Kasetsart University, Nakhon Pathom, Thailand
**Corresponding author; E-mail address: karun.kl@ku.ac.th*

Abstract

This paper presents the instability and post-buckling behaviors of the variable-arc-length (VAL) pipe caused by internal transporting fluid motion, including the effects of the pipe weight and variation of internal fluid pressure. The set of governing equation of the pipe, which is nonlinear first-order differential equation is derived by considering the equilibrium of force and moment and the geometric relation of the differential pipe segment in two-dimensions. The variation of internal pressure inside the pipe is calculated from the energy conservation based on Bernoulli principle. The set of governing equation corresponds to the two-point boundary value problem, which is conveniently solved by using the shooting method. The present numerical results are found to be compatible with the elliptic integral solution provided in the available literature. The numerical results indicate that the effects of the pipe and internal fluid weight are to decrease the critical buckling fluid velocity and cause to lose the pipe stability.

Keywords: Critical Velocity, Large Deflection, Nonlinear Frist-Order Differential Equation, Shooting Method, Variable-Arc-Length Pipe

1. Introduction

From the literature review, the problem of large deflection of variable-arc-length (VAL) elastica structure has been investigated by many researchers. Concerning with variable-arc-length beam, the research examples are presented by Theppitak [1], Rodsungwal [2], and Klaycham [3]. The span length of the variable-arc-length beam is a fixed distance, while the arc-length can be varied due to the external load. For this reason, the model of this structure type can be applied for pipe transporting crude oil in offshore structure applications. The problem of variable arc-length pipe was investigated by Chucheepsakul and Monprapussorn [4] using the elliptic integral method. They reported that the dimensionless critical internal fluid velocity of the VAL pipe for the first four modes are 9.8696, 39.4784, 88.8264, and 157.9137, respectively. Their numerical results have shown that the effect of elastic rotational restraint at support is to stabilize the pipe and to increase critical velocity. However, their mathematical model has not captured the effect of pipe weight and the variation of internal pressure along the pipe.

This study developed a mathematical model for analyzing of VAL pipe concerning the effect of pipe and internal fluid weight, internal fluid pressure, and compression force at the support. The set of nonlinear first-order differential equation of VAL pipe is derived by the considering equilibrium of force and moment. The numerical solution is solved by the shooting optimization method, which is found to be agreeable in comparing with the elliptic integral method presented by Chucheepsakul and Monprapussorn [4].

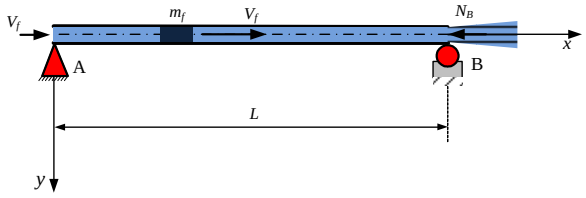

Fig. 1 The characteristic of variable arc-length pipe transporting fluid under applied compression at support B

2. Governing Equation and Numerical Method

Fig. 1 shows the schematic of variable-arc-length pipe transporting fluid in the two-dimensional Cartesian coordinate system (x , y). Both ends of the pipe are pinned support, which

located at the fixed position. The right end (point B) is subjected to a compression force (N_B) and can be slipped through the support. The span length is constant of length L , while total-arc-length (s_t) is an unknown length, which has to be investigated from the numerical solution.

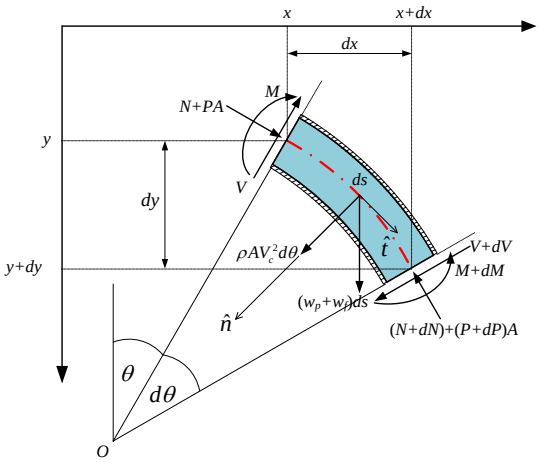

Fig. 2 Free body diagram of VAL pipe transporting fluid in effective system

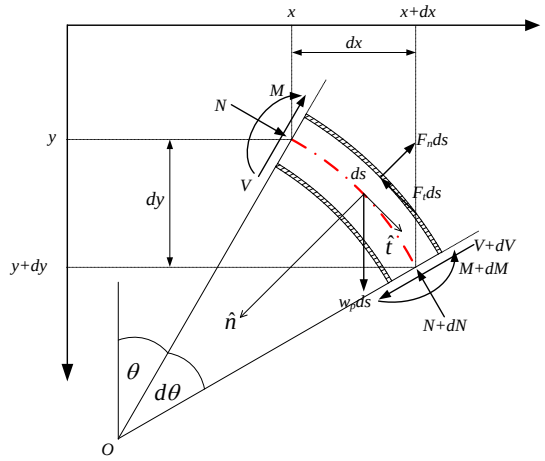

Fig. 3 Free body diagram of VAL pipe segment

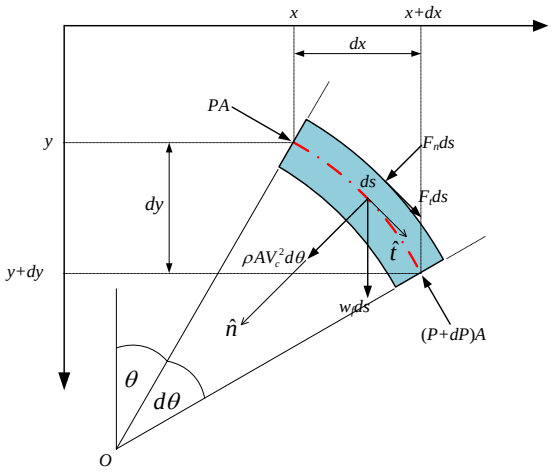

Fig. 4 Free body diagram of internal fluid segment

2.1 Geometric Relationship

Fig. 2 shows the free body diagram of a pipe transporting fluid in an effective system. Based on the differential geometry of the pipe segment with infinitesimal length (ds) in a plane curve, the geometric relations of the elastica pipe [5-6] can be expressed as follows.

$$\frac{dy}{ds} = \sin\theta \tag{1a}$$

$$\frac{dx}{ds} = \cos\theta \tag{1b}$$

$$\kappa = \frac{1}{r} = \frac{d\theta}{ds} = -\frac{M}{EI} \tag{1c}$$

where x and y are the horizontal and vertical coordinates; κ is the curvature of a pipe; r is the radius of curvature; θ is the angle measured from the horizontal direction to the tangent line of the pipe; M is the bending moment; and EI is the flexural rigidity of the pipe.

2.2 Equilibrium of Force and Moment

From the effective system of pipe segment shown in Fig. 2, it can be separated into the apparent systems of the pipe and the internal fluid as shown in Figs. 3 and 4, respectively. Considering the pipe segment, the equilibrium of force in tangential and normal directions are given in Eqs. (2a) and (2b); and the equilibrium of moment about point *O* can be given in Eq. (2c).

$$F_t = -\frac{dN}{ds} - V\frac{d\theta}{ds} + w_p \sin\theta \tag{2a}$$

$$F_n = \frac{dV}{ds} - N\frac{d\theta}{ds} + w_p \cos\theta \tag{2b}$$

$$\frac{dM}{ds} = V \tag{2c}$$

where F_t and F_n are the summation of fluid force in tangential and normal directions, respectively, acting on the pipe; w_p is the pipe weight per unit length; N , V , and M are the axial compression force, shear force, and bending moment, respectively. Similar to the above, considering Fig. 4, the equilibrium of force in tangential and normal directions of internal fluid segment are given in Eqs. (3a) and (3b), respectively.

$$F_t = A\frac{dP}{ds} - w_f \sin\theta \tag{3a}$$

$$F_n = PA\frac{d\theta}{ds} - \rho A V_c^{\,2}\frac{d\theta}{ds} - w_f \cos\theta \tag{3b}$$

in which $m_f = \rho A$ and $w_f = \rho A g$ are the mass and weight per unit length of internal fluid; V_c and ρ are the velocity and density of internal fluid; A is the inside cross-sectional area of the pipe; and g is the gravitational acceleration. To obtain the equilibrium equation of the effective pipe transporting fluid system, the method of superposition is applied to Eqs. (2) and (3). By equating Eq. (2a)=(3a) and Eq. (2b)=(3b), yield the Equilibrium of force in tangential and normal directions as given in Eqs. (4a) and (4b), respectively. Similarly, one obtains the moment equilibrium equation of the effective pipe system as given in Eq. (4c).

$$\frac{dN}{ds} = -V\frac{d\theta}{ds} - A\frac{dP}{ds} + \left(w_p + w_f\right)\sin\theta \tag{4a}$$

$$\frac{dV}{ds} = N\frac{d\theta}{ds} + PA\frac{d\theta}{ds} - \rho A V_c^{\,2}\frac{d\theta}{ds} - \left(w_p + w_f\right)\cos\theta \tag{4b}$$

$$\frac{dM}{ds} = V \tag{4c}$$

2.3 Variation of Internal Pressure

Considering internal pressure in Fig 4, when the internal fluid in the VAL pipe is moving it causes changes in internal pressure. Based on the energy conservation, the variation of internal pressure along the pipe can be calculated from the Bernoulli equation as follows.

$$\frac{dP}{ds} = \gamma\frac{dy}{ds} \tag{5}$$

where $\gamma = \rho g$ is the specific weight of the internal fluid.

2.4 Numerical Solution by Shooting Method

For convenience in the numerical computation, the set of first-order nonlinear differential equation should be written in nondimensional form, in which the following relations are used.

$$s^* = \frac{s_s}{s_t}, \hat{s}_t = \frac{s_t}{L}, \hat{x} = \frac{x}{L}, \hat{y} = \frac{y}{L} \tag{6a}$$

$$\hat{M} = \frac{ML}{EI}, \hat{P} = \frac{PAL^2}{EI}, \hat{w}_f = \frac{w_f L^3}{EI}, \hat{V} = \frac{VL^2}{EI} \tag{6b}$$

$$\hat{N} = \frac{NL^2}{EI}, \hat{w}_p = \frac{w_p L^3}{EI}, \hat{V}_c = \frac{\rho A V_c^2 L^2}{EI} \tag{6c}$$

where s^* and $\hat{s}_t$ are dimensionless arc-length coordinate and the total arc-length; $\hat{x}$ and $\hat{y}$ are dimensionless coordinate along horizontal and vertical directions; $\hat{w}_p$ and $\hat{w}_f$ are dimensionless pipe and internal fluid weights; $\hat{V}_c$ and $\hat{P}$ are dimensionless velocity and pressure of internal fluid; $\hat{M}$, $\hat{V}$, and $\hat{N}$ are bending moment, shear force, and axial compression force, respectively. Using Eq. (6), the set of governing equations of the pipe transporting fluid, including geometric relation (Eq. 1), equilibrium equation (Eq. 4), pressure variation (Eq. 5) can be transformed to dimensionless form as follows.

$$\frac{d\hat{x}}{ds^*} = \hat{s}_t \cos\theta \tag{7a}$$

$$\frac{d\hat{y}}{ds^*} = \hat{s}_t \sin\theta \tag{7b}$$

$$\frac{d\theta}{ds^*} = \hat{s}_t\hat{M} \tag{7c}$$

$$\frac{d\hat{V}}{ds^*} = \hat{N}\frac{d\theta}{ds^*} + \hat{P}\frac{d\theta}{ds^*} - \hat{V}_c\frac{d\theta}{ds^*} - \left(\hat{w}_p + \hat{w}_f\right)\hat{s}_t\cos\theta \tag{7d}$$

$$\frac{d\hat{N}}{ds^*} = \frac{d\hat{P}}{ds^*} - \hat{V}\frac{d\theta}{ds^*} + \left(\hat{w}_p + \hat{w}_f\right)\hat{s}_t\sin\theta \tag{7e}$$

$$\frac{d\hat{M}}{ds^*} = \hat{s}_t\hat{V} \tag{7f}$$

$$\frac{d\hat{P}}{ds^*} = \hat{w}_f\frac{d\hat{y}}{ds^*} \tag{7g}$$

Eqs. (7a)-(7g) are nonlinear first-order differential equations, which correspond to the two-point boundary value problem. Then the shooting optimization method is used to solve the numerical solution. From the support conditions, the coordinate of the left end support (point A) is located at $\hat{x}$ =0 and $\hat{y}$ =0, while the right support (point B) is at $\hat{x}$ =1 and $\hat{y}$ =0. Because the support is pinned, the bending moment at the pipe ends is

equal to zero. The inlet water pressure (point A) is specified according to the pump performance ($\hat{P} = \hat{P}_A$). Because both supports are at the same level and the water head loss is not considered, the outlet pressure is then equal to the inlet pressure ($\hat{P}_B = \hat{P}_A$). In the numerical implementation, the total arc-length ($\hat{s}_t$), which is the control variable is set the value. Then Eq. (7) is integrated from s^* =1 (point B) to s^* =0 (point A). Seven initial conditions at support B need to be given, which can be categorized into two groups. First is the specified condition such as $\hat{x} = 1$, $\hat{y} = 0$, $\hat{N} = \hat{N}_B$, $\hat{P} = \hat{P}_B$, and $\hat{M} = 0$. The second group is the unknown conditions including θ and $\hat{V}$, which have to guess firstly, as θ_B and $\hat{V}_B$, respectively. Also, the fluid velocity ($\hat{V}_c$) is unknown and will be guessed for the first iteration. At the upper limit of integration (point A), the specified boundary conditions ($\hat{x} = 0$, $\hat{y} = 0$, and $\hat{M} = 0$) should be set for the minimization process. Then the iteration process is repeated until the solution is satisfied the following objective function.

$$\underset{\theta_B, \hat{V}_B, \hat{V}_c}{\text{Min}} \; \Phi = \left|\hat{x}(0)\right| + \left|\hat{y}(0)\right| + \left|\hat{M}(0)\right| = 0 \qquad (8)$$

3. Numerical Results

3.1 Numerical Validation in Case of VAL Pipe without Effect of Pipe Weight and Internal Fluid Pressure

The numerical results obtained from the shooting method (SM) are checked with the result from the Elliptic integral method (EIM) presented by Chucheepsakul and Monprapussorn [4]. In this validation example, the effect of pipe and internal fluid weights ($\hat{w}_p = \hat{w}_f$ =0), and the inlet fluid pressure ($\hat{P}_A$ = 0) is not considered.

The load-displacement curve between the internal fluid velocity $(\hat{V}_c)$ and the support rotation at point B (θ_B) for the first four modes of VAL pipe are shown in Fig. 5. The numerical result shows that the pipe remains keeping undeformed shape until the fluid velocity reaches the maximum value at the critical state. At this state, the pipe is buckled. The maximum fluid velocity is called the critical buckling velocity. Beyond the critical state, the pipe is unstable and the post-buckling behavior occurs. At an unstable state, the support rotation is increased but the fluid velocity decreases. It is also found that the higher buckling mode requires a higher critical fluid velocity.

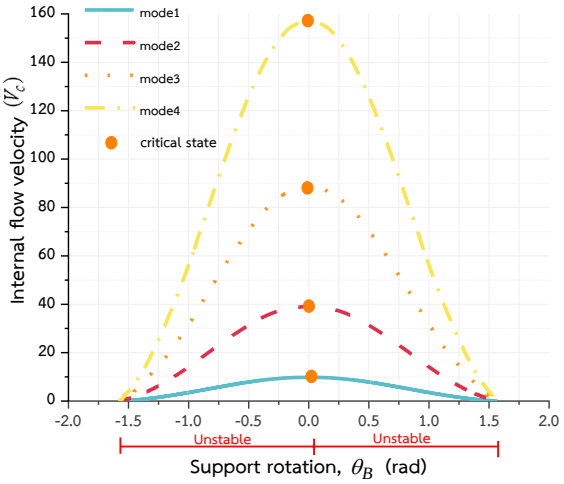

Fig. 5 Relations between internal fluid velocity ($\hat{V}_c$) and support rotation at point B (θ_B) for the first four buckling modes

The critical fluid velocity for the first four buckling modes of VAL pipe obtained in this study by using the shooting method (SM) is shown in Table 1. It is also compared with the results from the elliptic integral method (EIM) presented by Chucheepsakul and Monprapussorn [4]. The numerical results compared in Table 1 include the angle at support B (θ_B), the maximum deflection $(\hat{y}_{\max})$, the total arc-length $(\hat{s}_t)$, and the critical fluid velocity $(\hat{V}_{c\max})$. The critical velocity for the first four modes are found to be 9.869596, 39.476336, 88.780166, and 157.575295, respectively, which is agreeable with the result from EIM. Also, these critical values are acceptable with the theoretical buckling load of column derived from the linear analytical method, which equals to $n^2\pi^2$ (Exact solution), in which n is the buckling mode number.

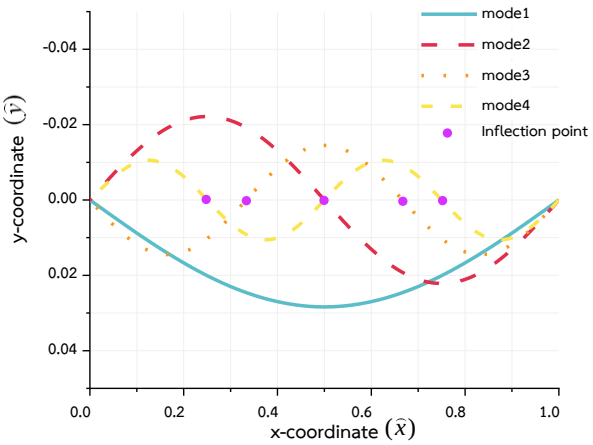

Fig. 6 Deformed shape of VAL pipe for the first four modes ($\hat{V}_c$ =5)

Table 1 Comparison of numerical result at critical state of VAL pipe for the first four deformed mode shapes ($\hat{w}_p$ = 0.00, $\hat{w}_f$ = 0.00, $\hat{P}_A$ = 0.00 and $\hat{N}_B$ = 0.00)

Mode	θ_B		$\hat{y}_{\max}$		$\hat{s}_t$		$\hat{V}_{c\max}$	
	EIM	SM	EIM	SM	EIM	SM	EIM	SM
1	0.000000	0.000000	0.000000	0.000000	1.000000	1.000000	9.869604	9.869596
2	0.000000	0.000000	0.000000	0.000000	1.000000	1.000000	39.478418	39.476336
3	0.000000	0.000000	0.000000	0.000000	1.000000	1.000000	88.826440	88.780166
4	0.000000	0.000000	0.000000	0.000000	1.000000	1.000000	157.913670	157.575295

The post-buckling configuration of the VAL pipe for the first four modes subjected to the same fluid velocity ($\hat{V}_c$ =5) are shown in Fig. 6. It is found that, at this velocity, there are at least four buckled shapes, which depend on the number of an inflection point. The number of inflections point for each buckling mode is found to be n -1.

3.2 Effect of Pipe Weight and Fluid Pressure Variation

This section presents the instability of VAL pipe including the effect of pipe and internal fluid weights, internal pressure, and compression at the support. In this example, internal fluid weight $(\hat{w}_f)$ is set to be 4, while the pipe weight $(\hat{w}_p)$, the inlet fluid pressure $(\hat{P}_A)$, and the compression force at the support B $(\hat{N}_B)$ are specified to be 2.

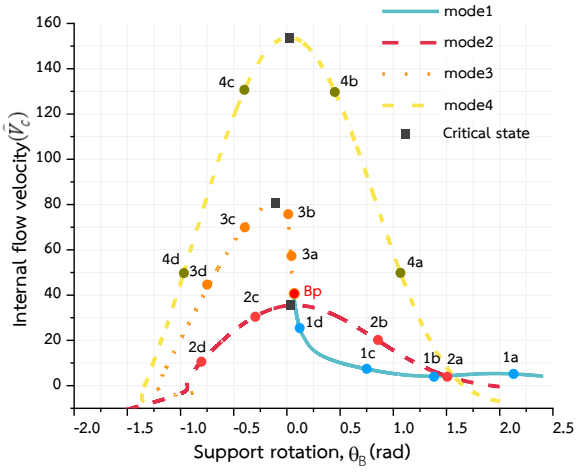

Fig. 7 Relations between internal fluid velocity ($\hat{V}_c$) and support rotation at point B (θ_B) for the first four buckling modes

The relations between the fluid velocity ($\hat{V}_c$) and the support rotation at point B (θ_B) for the first four modes of VAL pipe are shown in Fig. 7. As shown in this figure, the 1st mode obeys only unstable behavior, where the support rotation increases by decreasing the fluid velocity. The deformed shape becomes the 3rd mode when the fluid velocity reaches the transition point (Bp). For the 3rd mode, the fluid velocity is suddenly increased until it passes the point Bp and approaches the critical state. The maximum or critical velocity can be found from the critical state, which is equal to 81.429640. Beyond the critical state, the fluid velocity is decreased by increasing the support rotation. The post-buckling behavior of the 2nd and the 4th modes are the same, but the critical velocity of the 2nd mode is lower than the other one. The critical velocity of the 2nd and the 4th modes are found to be 35.506625 and 154.239955, respectively.

The deformed shape for the first four buckling modes along the load-displacement curve in Fig. 7 are shown in Figs. 8-11, respectively (the abbreviations 1a, 1b, 1c, ..., and 4d are represented the point on the curves in Fig. 7). It is found that the number of inflections point for each buckling mode is found to be n -1, which is agreeable with the earlier result in previous section.

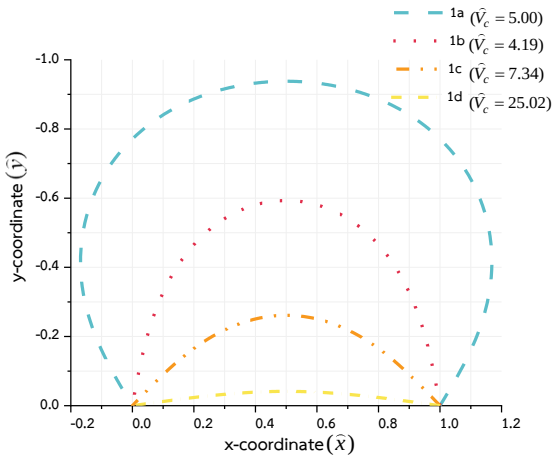

Fig. 8 Buckled shape of the 1st mode of VAL pipe for various fluid velocities

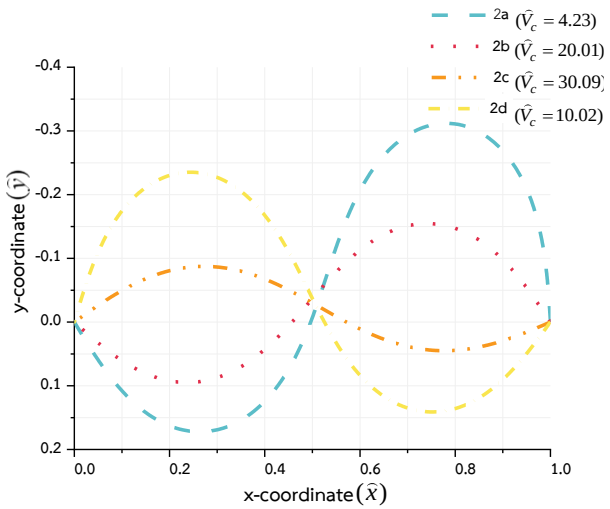

Fig. 9 Buckled shape of the 2nd mode of VAL pipe for various fluid velocities

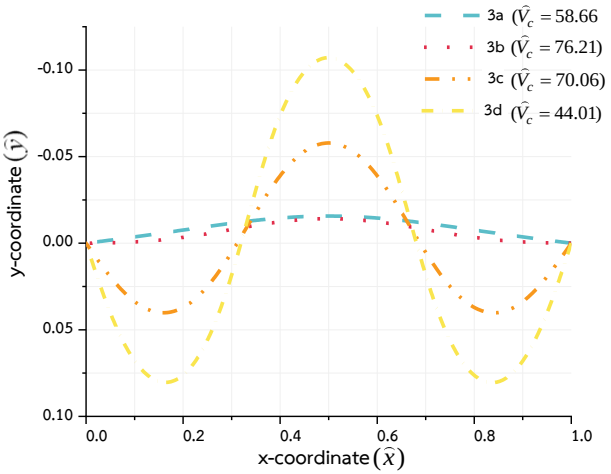

Fig. 10 Buckled shape of the 3rd mode of VAL pipe for various fluid velocities

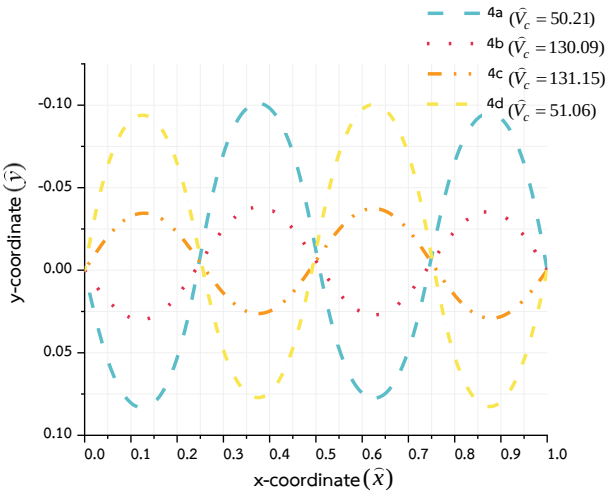

Fig. 11 Buckled shape of the 4th mode of VAL pipe for various fluid velocities

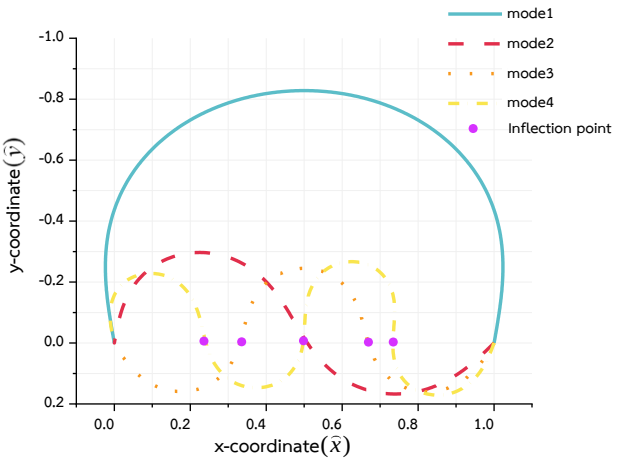

Fig. 12 Buckled shape of VAL pipe for the first four modes ($\hat{V}_c$ =5)

Fig. 12 shows the first four buckled configuration under the same fluid velocity of $\hat{V}_c$ =5. Based on the buckled shapes in Fig. 12, the distributions of shear force $(\hat{V})$, bending moment $(\hat{M})$, axial force $(\hat{N})$, and the internal fluid pressure $(\hat{P})$ along the arc-length coordinate (s^*) are shown in Figs. 1 3 -16 , respectively. We find that the maximum shear force is located at the inflection point. The bending moment and axial compression force are maximum at the highest or lowest points on the buckled shape. However, the maximum internal pressure is located at the lowest point on a buckled shape, while the minimum pressure is located at the highest point on the buckled shape.

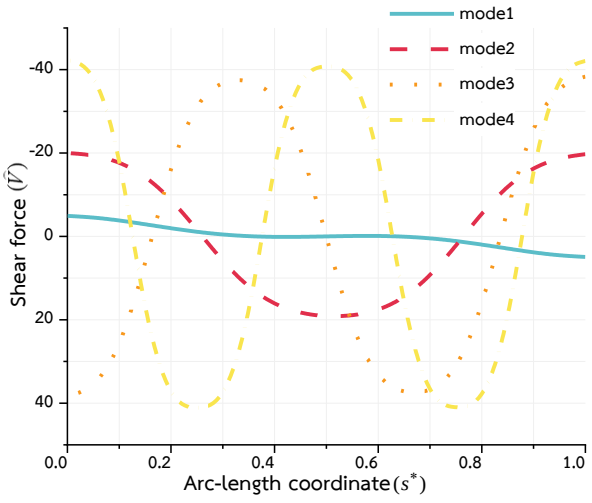

Fig. 13 Distribution of shear force $(\hat{V})$ along arc-length coordinate (s^*) for the first four modes ($\hat{V}_c$ =5)

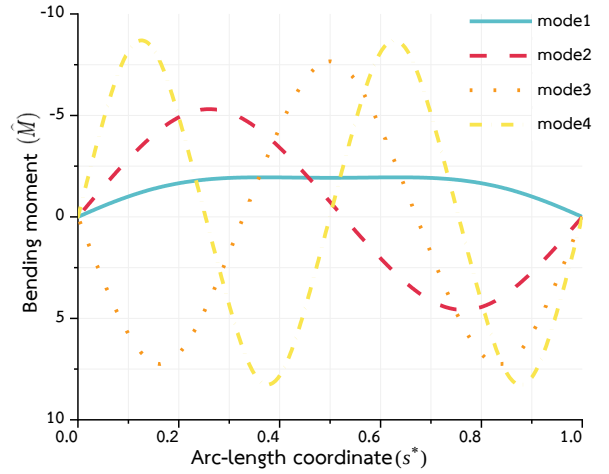

Fig. 14 Distribution of bending moment $(\hat{M})$ along arc-length coordinate (s^*) for the first four modes ($\hat{V}_c$ =5)

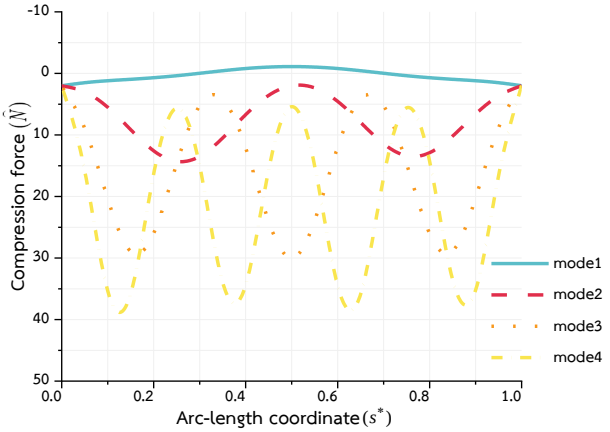

Fig. 15 Distribution of axial force $(\hat{N})$ along arc-length coordinate $(\hat{s}^*)$ for the first four modes ($\hat{V}_c$ =5)

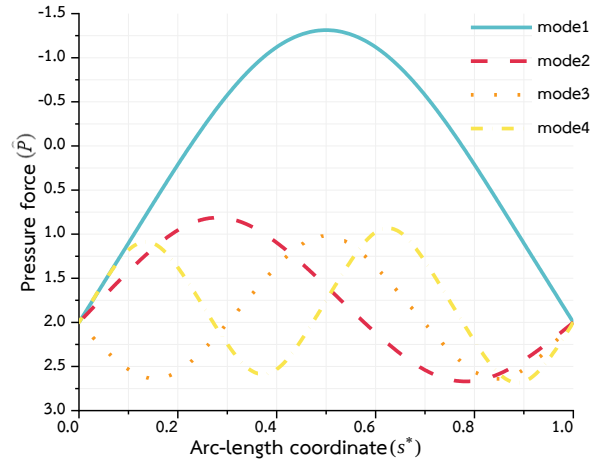

Fig. 16 Distribution of internal pressure $(\hat{P})$ along arc-length coordinate (s^*) for the first four modes ($\hat{V}_c$ =5)

4. Conclusions

This paper presents the large deflection of VAL pipe including the effect of pipe and internal fluid weights, internal pressure, and compression force at the support. The set of governing first-order differential equations of pipe is derived from the geometric relation and the equilibrium equation. Based on energy conservation, the variation of internal pressure is calculated from the Bernoulli equation. The numerical solution is solved by using the shooting method. The presented numerical results are found to be agreeable with the result from the elliptic integral method provided in the literature. Without the effect of pipe and internal fluid weight, the buckling behavior of a pipe under the centrifugal force of internal fluid behaves the theoretical buckling column behavior. The dimensionless maximum or critical fluid velocity is approached $(n\pi)^2$, in which n is the buckling mode number. Beyond the buckling state, the pipe obeys unstable behavior. Including the effect of pipe and internal fluid weights, internal pressure, and compression force at support, the buckled path of the 1st mode can be transited to the 3rd mode.

Acknowledgement

The authors would like to thank the Department of Civil Engineering, Faculty of Engineering at Kamphaeng Saen, Kasetsart University for the financial support and the necessary facilities in this study.

References

[1] Theppitak, G. (1995). *Large Deflection Analysis of Simple Variable-Arc-Length Beam under Various Loading Condition*. King Mongkut's University of Technology Thonburi, Thailand.

[2] Rodsungwal, S. (1999). *Large Deflections Analysis of Variable-Arc-Length Beams via the Finite Element Method*. M.Sc. Thesis, King Mongkut's University of Technology Thonburi, Thailand.

[3] Klaycham, K. (2019). Critical Self-Weight of Inclined Variable-Arc-Length Beam under Applied Tension at Support, *KMUTT Research and Development Journal*, Vol. 42, No. 3, pp. 263-278. (In Thai)

[4] Chucheepsakul, S. and Monprapussorn, T. (2000). Divergence Instability of Variable-Arc-Length Elastica Pipes

Transporting Fluid. *Journal of Fluid and Structures*, Vol.14, pp.895-916.

[5] Gormann, D.G., Reese, J.M. and Zhang, Y.L. (2000). Vibration of a Flexible Pipe Conveying Viscous Pulsating Fluid Flow. *Journal of Sound and Vibration*, Vol.2, pp.379-392

[6] Klaycham, K., Athisakul, C., and Chucheepsakul, S. (2014). Finite Element Method for Critical Top Tension Analysis of Neutrally Buoyant Riser. *KMUTT Research and Development Journal*, Vol.4, pp.429-446.